AIAA-98-0436

Measurements of Controlled Wave Packets at Mach 4 on a Cone at Angle of Attack

Dale W. Ladoon and Steven P. Schneider

Scool of Aeronautics and Astronautics
Purdue University
West Lafayette, IN 47907-1282

36th Aerospace Sciences Meeting & Exhibit

January 12-15, 1998 / Reno, NV

Measurements of Controlled Wave Packets at Mach 4 on a Cone at Angle of Attack

D.W. Ladoon* and S.P. Schneider†
School of Aeronautics and Astronautics
Purdue University, West Lafayette, IN 47907-1282

ABSTRACT

An experimental study of wave-packet development on a sharp-nosed, 5° half-angle cone was conducted in a Mach 4, quiet-flow wind tunnel. The cone was pitched to a 3° angle of attack. Controlled and repeatable disturbances were created at the wall of the laminar boundary layer by a pulsed, point-source, glow-discharge. Flow measurements were made along the leeward ray of the cone with a single-element, hot-wire probe. Boundary-layer traverses were made at three locations downstream of the glow to characterize the streamwise evolution of the wave packet.

The peak wave amplitude occurred near the boundary-layer edge and in the region of maximum shear. The boundary-layer thickness at the furthest streamwise measurement station of x = 140 mm (Re_x = 570,000) was about 5.6 mm. Weak but significant wave growth was observed. The convective speed of the packet was on the order of 0.89 times the freestream velocity. Repeatability of the wave packet is 4.5 percent based on the peak rms amplitude .

1.0 INTRODUCTION

An understanding of laminar-turbulent transition in high-speed boundary-layers is important for design of supersonic and hypersonic vehicles. Transition affects both skin friction and heat transfer and, hence, performance parameters such as drag and structural heat loads. Despite recent progress in theoretical and numerical modeling, the mechanisms leading to high-speed transition are still poorly understood[16,17]. Therefore, more experimental data, in the form of boundary-layer stability measurements, are needed to assist in the development of theory and computations.[23]

Although flight vehicles are generally three-dimensional and fly at angle of attack, most measurements of high-speed boundary-layer instabilities have been made on symmetrical geometries such as flat plates and round cones at zero angle of attack. The crossflow instability, which may be dominant in many three-dimensional (3D) geometries, only appears in 3D flowfields. One of the simplest geometries, which exhibits 3D supersonic boundary-layer flow, is a round cone at angle of attack (AOA). Transition on high-speed cones at AOA has been the subject of many studies. The majority of these experiments have consisted of surface measurements, typically using thermocouples or hot-films, to determine the location of the transition front. Notable studies where instability measurements have been made on sharp cones at AOA are the Mach 8 experiments of Stetson et al.[22], the Mach-6 quiet-tunnel experiments of Doggett et al.[3], and the Mach 3 experiments of Olsson[15]. Further references and details on transitional boundary layers over sharp cones at AOA are given in References [13] and [18].

In contrast to subsonic investigations, the interpretation of most high-speed transition experiments has been ambiguous due to the lack of a low disturbance, or quiet, environment and to poorly characterized disturbance fields. For example, most high-speed experimental work has been conducted in conventional facilities where freestream disturbances are large due to eddy-Mach-wave acoustic radiation from the normally turbulent boundary layers on the wind-tunnel side walls[2, 10]. Furthermore, most of these investigations have studied natural transition caused by uncontrolled and poorly characterized disturbance fields.

Instability and transition is best characterized by using controlled, or artificial, disturbances that are introduced into a laminar flow to excite instabilities or to create turbulence. Measurements can then be synchronized with the disturbance source[5,9]. Two classic examples are the flat-plate, vibrating-ribbon experiments of Schubauer and Skramstad[21] in low-speed flow and the flat-plate, glow-discharge experiments of Kendall[7,8] in high-speed flow. Glow-discharges have also been used by other researchers to generate controlled perturbations in high-speed laminar flows.[4,14] The main advantage of the glow-discharge technique is that one can easily control the amplitude and frequency of the perturbations. Furthermore, the discharge is capable of creating high-frequency perturbations.

---

* Graduate Research Assistant, Student Member AIAA

† Associate Professor, Senior Member AIAA

For natural transition in the typically low-disturbance environment encountered in flight, disturbances excite a broad spectrum of waves in a laminar boundary layer.[1,5,6,8] This leads to modulated wave trains whose constitutive elements have different frequencies and wave numbers[6]. A controlled approach to studying the problem, which emulates natural transition, is to generate a wave packet via a localized pulse. A pulsed point source excites a wide band of frequencies and wave numbers simultaneously in the flow. The boundary layer then selectively amplifies those waves which are most unstable.[6, 8]

In this paper, Mach-4 quiet-flow wind-tunnel experiments are presented in which controlled perturbations were used to create wave packets in the laminar boundary-layer of a 5° cone at 3° angle of attack. Localized perturbations were produced at the surface of the model by a pulsed glow discharge.

2.0 EXPERIMENTAL APPARATUS

2.1 Test Facility

This experimental study was conducted in the Mach-4, Purdue Quiet-Flow Ludwieg Tube (PQFLT). The PQFLT is a short-duration wind tunnel with a run time of approximately 3.5 seconds. The stagnation pressure and temperature decrease by approximately 35 and 10 percent, respectively, during the 3.5 second run time[20]. However, as described in Reference [20], the flow is quasi-steady for consecutive intervals of 121 msec. For the results presented in this paper, the wind tunnel stagnation pressure and temperature were about 77 kPa and 287 K. The corresponding unit Reynolds number in the test core is on the order of 37,000/cm.

Within the inviscid core flow of the nozzle is a test rhombus of uniform quiet flow. Pitot-probe measurements along the tunnel axis show that the rms total pressure fluctuations in the test-core flow are about 0.05 percent for stagnation pressures less than 83 kPa. This corresponds to noise levels which are typically an order of magnitude less than those of conventional facilities.[19]

2.2 Test Model and Measurement Instrumentation

The test model, shown in Figure 1, is 152-mm long and made of steel. The first 145 mm of the model consists of a straight, 5° half-angle cone. The cone smoothly tapers to a 25.4-mm diameter cylinder for the remaining 7 mm of the model. The tip radius is less than 0.006 mm, so bluntness effects are not expected to be a factor. The surface is polished to an RMS surface roughness of less than 0.05 μm. The cone was mounted to the wind tunnel via a 23.7-mm diameter sting. The face of the sting was machined at an angle of 3° with respect to its axis to place the cone at 3° AOA.

Boundary-layer measurements were made using a TSI IFA100, constant temperature anemometer (CTA) and a single-element hot-wire probe. The hot-wire voltage signal was acquired by a LeCroy 9304AM digital oscilloscope. The anemometer was operated in the 1:1 bridge mode. The signal conditioner applied a gain of 2 and low-pass filtered the signal at a cut-off frequency of 400 kHz. The custom-built probe consists of a 0.0038-mm diameter Tungsten sensing element mounted between two 0.076-mm diameter steel needles which are spaced 0.51 mm apart. The corresponding wire aspect ratio, l/d, is 133. The hot-wire was operated at an overheat of 0.95 and the frequency response was typically 155 kHz. The probe was mounted to a two-dimensional traverse via a sting and double-wedge strut assembly. The vertical position, y, of the hot-wire sensing element was measured optically using a long-distance microscope. The maximum uncertainty in the vertical position is ± 0.06 mm.

The position of the hot-wire probe is fixed for a given wind tunnel run. Therefore, data points at different boundary-layer locations are obtained by making multiple runs and repositioning the hot-wire for each run. In general, to obtain a boundary-layer profile, the streamwise position, x, of the probe is fixed. The vertical position of the hot-wire, y, is then varied in a random fashion so that any systematic errors can be detected. For example, if the hot-wire was originally close to the wall, the next measurement would be made further from the wall, the following position would then be closer to the wall, and so on.

2.3 Glow-Discharge Perturber

Controlled, localized, and repeatable perturbations were produced at the surface of the cone by a point-source, glow discharge. This was accomplished by applying a voltage potential between two flush-mounted, concentric electrodes. The electrode configuration is shown in Figure 1. At a sufficiently high voltage, the air surrounding the tip of the electrodes ionizes, and an electrical discharge, or plasma, is established. This plasma creates density and temperature disturbances due to the accompanying resistive, or Joule, heating of the air. The discharge is visible as a distinctive blue glow of plasma around the electrodes. A photograph of a glow-discharge on the 5° cone in Mach-4 flow is shown in Figure 2.

The electronics used to produce a glow discharge were custom built and are described in References [11]

and [12]. The voltage signal across the electrode gap was measured with a Tektronics P5200 high-voltage differential probe. This signal served as a reference for triggering the oscilloscope and for ensemble averaging the hot-wire signals.

The hot-wire is susceptible to electronic, or radio frequency (RF), noise emitted from the glow discharge. However, this does not present too much of a problem when the glow is used as a pulsed source. Specifically, useful flow measurements can be made if the pulse is relatively short and the hot-wire is adequately far downstream of the electrodes. The rationale for this is that once the glow is turned off, any perturbations measured in the flow must be real and not a manifestation of RF noise from the glow.

The glow-discharge electronics allow for various types of AC excitation wave forms, including rectified signals. However, for the data reported in this paper, the input waveform to the electrodes consisted of the negative portion of a four-cycle sine wave. Referring to Figure 1, the inner 18 AWG copper electrode is then the cathode. The effect of electrode polarity on the glow and the type of flow perturbations generated will be described in Reference [12]. In Reference [11], the present authors reported that negative pulses resulted in arcing. It was later found that this was due to a crack in the ceramic.

3.0 EXPERIMENTAL RESULTS

The 5°-cone can be rotated and fastened in its sting to place the center of the electrodes at any desired azimuthal location. However, for this study, the center of the concentric electrodes was aligned with the leeward ray. All flow measurements were made along the leeward ray and downstream of the electrodes. The hot-wire was not calibrated and only the anemometer bridge voltage, e, is reported. Due to the high overheat, the hot-wire is expected to be primarily sensitive to mass-flux fluctuations.

The input pulsed waveform to the electrodes consisted of the negative portion of a four-cycle, 50 kHz sine wave. Limited data at other input frequencies has already been collected and will be given in Reference [12]. The input voltage was fixed, resulting in an RMS voltage drop across the electrodes of 590 ± 5 V. Since the glow voltage was consistent for each wind tunnel run, it is assumed that resulting perturbations were the same. A typical trace of the voltage drop across the electrodes, V_g, for a pulsed glow discharge on the 5° cone in Mach-4 flow is shown in Figure 3(a).

For each wind tunnel test, the hot-wire signal was acquired using two LeCroy 9304AM digital oscilloscopes. One oscilloscope was operated in continuous mode, collecting data at a sampling frequency of 250 kHz for 1 second. This oscilloscope was triggered by the start of the wind tunnel. The other oscilloscope acquired 248 data segments, or records, which were each 1000 points in length. The sampling frequency for the segmented data was 2 MHz, which gives a record length of 0.5 msec. Each segment was triggered by the voltage pulse in the electrode gap. The interval between pulses, as set via the input signal from the function generator to the glow-discharge circuit, was 1.02 msec. The DC-coupled continuous data was used to determine the mean boundary-layer profiles. The AC-coupled segmented data recorded the wave packets created by the glow discharge.

A new triggering system was devised for this study to start the glow at a specified time after the start of the wind tunnel. Once the glow is triggered, a fixed number of pulses are generated at specified intervals. The glow pulses in turn trigger the segmented oscilloscope. The primary advantage of specifying a time delay to start the glow is that it allows one to maintain consistent freestream flow properties between runs. This adds to the repeatability of an experiment. For instance, the glow can be regularly started at the beginning of one of the 121 msec. quasi-steady periods that occur during the 3.5 second run time of the wind tunnel. During these quasi-steady periods, the tunnel unit Reynolds number, Re_{unit}, and the ratio of the cone wall to freestream stagnation temperature, T_w/T_o, are nearly constant. For the 3° AOA data reported in this paper, a glow was initiated 640 msec. after the start of the wind tunnel.

The hot-wire signals from the segmented data were ensemble averaged to remove uncorrelated noise. 248 segments were collected for each run. The first ten segments were discarded, since the glow occasionally takes a few pulses to stabilize and become repeatable. The following 70 segments were then ensemble averaged. The remaining 148 segments spanned over the next quasi-steady time period where the tunnel Reynolds number was 1.2 % lower and the ratio of the cone wall to freestream stagnation temperature was 1.1 % higher. In order to minimize such effects, these segments were not used. Typical single realization and ensemble averaged hot-wire traces are given in Figures 3(b), (c), and (d). The large amplitude spikes from t = 0 to 0.85 msec. is RF noise from the glow. A wave packet is observed at a later time, t = 0.130 msec., after the glow has been turned off. The traces in Figures 3(b), (c), and (d) were measured at a streamwise distance of x = 140 mm and a wall-normal distance of 5.15 mm.

3.1 Mean Flow

Laminar boundary-layer profiles measured on the cone at 3° AOA are shown in Figure 4(a). The profiles at x = 125 mm and 140 mm are relatively complete, while only a partial profile was taken at x = 112 mm. For comparison, a boundary-layer profile with the cone at zero AOA and at x = 141 mm is included in Figure 4(a). The zero AOA data was obtained at a slightly higher tunnel unit Reynolds number of 37800/cm, which is only 2.2 % greater than that of the AOA data. Clearly, the boundary-layer thickness at AOA is substantially larger than at zero AOA. This is due to the three-dimensional nature of the flow over the cone when it is placed at AOA. Specifically, crossflow directed from the windward to the leeward side of the model, results in a "swelling" of the boundary layer at the leeward ray. At 3° AOA and x = 140 mm, the boundary-layer thickness, δ, is 5.6 mm. This is 2.6 times the value measured at zero AOA and x =141 mm.

Non-dimensional profiles of the data shown in Figure 4(a) are given in Figure 4(b). The vertical position, y, is scaled by the square root of the local streamwise distance from the tip, x. In order to match the boundary-layer edge of the zero AOA profile with those of the AOA profiles, the zero AOA data has been multiplied by a factor of A = 2.6. This value corresponds to the ratio of δ at 3° AOA to δ at zero AOA. The AOA profiles collapse reasonably well, which suggests a degree of similarity on the leeward ray. All the profiles are markedly inflectional near the outer edge of the boundary layer. However, the crossflow at AOA results in a profile with a narrower and sharper "high-shear" region. As a result, one expects the AOA boundary layer to be more unstable.

3.2 Mode Shapes

Measurements of the perturbation created by the pulsed glow discharge were made downstream of the electrodes. The hot-wire probe was traversed through the boundary-layer at streamwise locations of x = 112 mm, 125 mm and 140 mm. The distribution of the perturbation amplitude across the boundary layer is shown in Figure 5(a). Note that e'_{RMS} is the root-mean square (RMS) value of the wave packet (WP) generated by the glow discharge. Typical WPs are shown in the hot-wire fluctuation traces, $e'(t)$, of Figures 3, 6, and 8. The leading and trailing edges of the WP were determined based on a slope, de/dt, criterion. Details on the RMS calculation of the WP will be provided in Reference [12].

From Figure 5(a), the amplitude of the WP changes with boundary-layer height. In particular, the amplitude is zero near the wall and in the freestream. Furthermore, the perturbation is primarily confined to the outer portion of the boundary layer. The peak amplitude occurs in the high-shear region near the inflection point. This is more clearly visible in Figure 5(b), where the vertical distance has been non-dimensionalized by the square root of the streamwise distance from the model tip. As with the mean profiles shown in Figure 4(b), the locations of the peak amplitudes collapse quite well.

The vertical extent of the disturbance broadens and the peak amplitude monotonically increases as the WP propagates downstream. This indicates that the WP is growing due to the instability of the boundary layer. The maximum measured disturbance amplitude at x = 140 mm is e'_{RMS} = 26.9 ± 1.2 mV. The ratio of this RMS fluctuation value to the mean-flow value at the boundary-layer edge is

$$\frac{e'_{RMS}}{e_{\delta}} = 0.8\ \% \quad .$$

It is important to recognize that since the hot-wire is uncalibrated, such ratios based on raw voltage values are not necessarily the same as those based on mass-flux values.

3.2.1 Repeatability

Repeatability of the glow perturber and the WP results was assessed by performing multiple wind tunnel runs with the hot wire at a fixed position of (x, y) = (140 mm, 5.03 mm). This location was chosen in order to provide the largest signal to noise ratio.

Ensemble averaged hot-wire fluctuation traces, e', at (x, y) = (140 mm, 5.03 mm) for four runs on three different days are plotted in Figure 6. The glow pulse starts at t = 0.0 msec. and ends at t = 0.08 msec., so the large amount of electronic noise on the hot-wire trace from t = 0 to about 0.90 msec. is RF pickup from the glow. The disturbance created by the glow convects downstream from the electrodes and a WP is observed at around t = 0.125 msec. Comparing the traces in Figure 6, it is clear that the WPs maintain the same shape and convection time. Interestingly, the WP has multiple peaks and the overall shape, or envelope, is not Gaussian. The dual-peaked nature of the waves may be due to the presence of harmonics and/or the waves may be non-linear. Further work is needed to access the type of perturbation and the linearity of the WP produced by the glow. Specifically, the amplitude and waveform of the input voltage signal to the electrodes can be varied. The effect on the resulting WP can then be measured with a hot-wire.

The WPs shown in Figure 6 are plotted on top of each other in Figure 7. Note that the peaks coincide, which indicates the wave packets have the same

convection time and phase. RMS values for the WPs are listed in Table 1. The mean value is 26.9 ± 1.2 mV, which gives a repeatability of approximately 4.5 %.

3.2.2 Wave-Packet Growth

Ensemble averaged hot-wire traces at streamwise locations of x = 112 mm, 125 mm, and 140 mm are shown in Figure 8. The vertical coordinate, y, for each plot corresponds to the respective peak amplitude in the mode shapes shown in Figures 4(a) and 4(b). Figure 8 clearly illustrates the increase in WP amplitude with downstream distance. This indicates WP growth. The RMS amplitudes of the WPs shown in Figure 8(a), (b), and (c) are 11.8 mV, 18.5 mV, and 27.4 mV, respectively. Using the value at x = 112 mm, the RMS ratios at x = 125 mm and x = 140 mm are

$$\frac{(e'_{\mathrm{RMS}})_{125\mathrm{mm}}}{(e'_{\mathrm{RMS}})_{112\mathrm{mm}}} = 1.57$$

and

$$\frac{(e'_{\mathrm{RMS}})_{140\mathrm{mm}}}{(e'_{\mathrm{RMS}})_{112\mathrm{mm}}} = 2.45 \ .$$

These ratios indicate the WP growth is significant but still small over the region that can be studied in the present facility.

3.2.3 Wave-Packet Convective Speed

The convective speed, c, of the wave packet can be estimated from the distance and time differences, Δx and Δt, between the peaks labeled 1, 2, and 3 in Figure 8. The corresponding values are c_{12} = 613 ± 24 m/s, c_{23} = 568 ± 19 m/s, and c_{13} = 588 ± 11 m/s. The subscripts denote the peaks that the calculations are based on. The uncertainty in the convective speed is due primarily to the uncertainty in Δx. The average value is 589 m/s. Since the freestream velocity is about 663 m/s, this gives a ratio of convective speed to freestream velocity, c/U_∞, of 0.89. This value is consistent with those of first and second mode instability waves in high-speed boundary layers.

Since the uncertainty in the convective speeds is significant, it is unclear if the high value between x = 112 mm and 125 mm is a real flow effect. For instance, the larger convective speed near the glow could be a near-field effect of the perturbation source. Further measurements well downstream of the electrodes are needed to access the near-field effects of the glow perturbation. This was not an option in the present study, since the maximum useful downstream measurement location is limited by the extent of the quiet-flow region in the nozzle.

4.0 CONCLUSIONS

A pulsed, surface glow-discharge was used to create measurable wave packets on the leeward ray of a 5° half-angle cone at 3° AOA. Mean-flow measurements show that crossflow results in a boundary layer at x = 140 mm (Re_x = 570,000) that is about 2.6 times thicker than that at zero AOA. The non-dimensionalized mean-flow profiles appear to be self-similar at 3° AOA. Mode shapes of the wave packet show that the disturbance resides in the outer portion of the boundary-layer where a high-shear region exists. The repeatability of the peak RMS amplitude in the mode shape was 4.5%. Wave packet growth was found to be significant but weak. Perhaps larger disturbance growth rates could be obtained by rotating the electrodes to a different azimuthal location to excite cross-flow instability. The average convective speed of the wave packet was 0.89 times the freestream velocity. The convective speed was highest near the glow electrodes. It is unclear if this is to due a near-field effect of the perturbation source.

The glow-discharge system used in this study proved to be a reliable and versatile means of producing controlled and repeatable perturbations in a high-speed, short-duration wind tunnel. As a result, this technique is now available for use in the new Mach-6 wind tunnel that is currently under construction at the Aerospace Sciences Laboratory of Purdue University.

ACKNOWLEDGMENTS

This work has been funded in part by the Air Force Office of Scientific Research under Grants F49620-94-1-0067 and F49620-97-1-0037 once monitored by Dr. L. Sakell and now Dr. S. Walker. Additional funding has been provided by a fellowship from the Purdue Research Foundation, a gift in memory of K.H. Hobbie, and a gift from the Boeing Company. The assistance of Dr. J.M. Kendall, from JPL, and Dr. A.D. Kosinov, from ITAM (Novosibirsk, Russia), in the development of the glow-discharge perturber is gratefully acknowledged. The authors would like to thank Don Bower, Madeline Chadwell, Joe Zachary, and, especially, Jim Younts for their high quality craftsmanship. The assistance of Terry R. Salyer in photographing the glow-discharge was also much appreciated.

REFERENCES

[1] Balakumar, P., and Malik, M.R., 1992, "Waves produced from a harmonic point source in a

supersonic boundary-layer flow, " *J. Fluid Mech.*, Vol. 245, pp. 229-247.

[2] Beckwith, I.E., and Miller, C.G., 1990, "Aerothermodynamics and transition in high-speed wind tunnels at NASA Langley," *Annual Rev. Fluid. Mech.*, Vol. 22, pp. 419-439.

[3] Doggett, G.P., Chokani, N., and Wilkinson, S.P., 1997, "Effect of Angle of attack on Hypersonic Boundary-Layer Stability," *AIAA Journal*, Vol. 35, No. 3, pp. 464-470.

[4] Ermolaev, Yu.G., Kosinov, A.D., and Semionov, N.V., 1996, "Experimental investigation of laminar-turbulent transition process in supersonic boundary layer using controlled disturbances," In *Nonlinear Instability and Transition in Three-Dimensional Boundary Layers*, pp.17-26, Kluwer Academic Publ.

[5] Gaster, M., and Grant, I., 1975, "An experimental investigation of the formation and development of a wave packet in a laminar boundary layer", *Proc. R. Soc. Lond. A.*, Vol. 347, pp. 253-269.

[6] Gaster, M., 1981, "Propagation of Linear Wave Packets in Laminar Boundary Layers," *AIAA Journal*, Vol. 19, No. 4, pp. 419-423.

[7] Kendall, J.M., 1967, "Supersonic Boundary Layer Stability Experiments," In *Proc. of Transition Study Group*, Vol. 2, W.D. McGauley (ed.), Aerospace Corp., San Bernardito, CA. (see also Kendall 1995)

[8] Kendall, J.M., 1995, "Experimental Methods and Results on Supersonic Boundary-Layer Stability and Receptivity," To appear in the *Proceedings of an ICASE/NASA LaRC Short Course,* Oxford University Press.

[9] Kosinov, A.D., Maslov, A.A., and Shevelkov, S.G., 1990, "Experiments on the stability of supersonic laminar boundary layers." *J. Fluid Mech.*, Vol. 219, pp. 621-633.

[10] Lachowicz, J.T., Chokani,, N., and Wilkinson, S.P, 1996, "Boundary-Layer Stability Measurements in a Hypersonic Quiet Tunnel," *AIAA Journal*, Vol. 34, No. 12, pp. 2496-2500.

[11] Ladoon, D.W., and Schneider, S.P., 1997, "Instability and Transition Experiments at Mach 4 using an Electrical-Discharge Perturber," *FEDSM* 97-3112. 1997 ASME Fluids Engineering Division Summer Meeting, June 22-26, Vancouver, B.C.

[12] Ladoon, D.W., 1998, "Waves Packets Generated by a Surface Glow Discharge on a Mach-4 Five Degree Cone at Zero and Three Degrees Angle of Attack," Ph.D. Dissertation, School of Aeronautics and Astronautics, Purdue University. (to appear)

[13] Malik, M., and Balakumar, P., 1992, "Instability and Transition in Three-Dimensional Supersonic Boundary Layers," *AIAA Paper* 92-5049.

[14] Martens, S., Kinzie, K.W., and McLaughlin, D.K., 1996, "Structure of Coherent Instabilities in a Supersonic Shear Layer," *AIAA Journal*, Vol. 34, No. 8, pp. 1555-1561.

[15] Olsson, J., 1996, "Experimental Hypersonic Transition Research: Summary of experimental cone transition research," *Aeronautical Research Institute of Sweden* Technical Report, FFA TN 1996-18.

[16] Reed, H.L., and Saric, W.S., 1996, "Linear Stability Theory Applied to Boundary Layers," *Ann. Rev. Fluid Mech.*, Vol. 28, pp. 389-428.

[17] Reshotko, E., 1994, "Boundary Layer Instability, Transition and Control, *AIAA Paper* 94-0001.

[18] Schmisseur, J.D., Schneider, S.P., and Collicott, S.H, 1998, "Receptivity of the Mach-4 Boundary-Layer on an Elliptic Cone to Laser-Generated Localized Freestream Perturbations," *AIAA Paper* 98-0532.

[19] Schneider, S.P., and Haven, C.E., 1995, "Quiet-Flow Ludwieg Tube for High-Speed Transition Research," *AIAA Journal*, Vol. 33, pp. 688-693.

[20] Schneider, S.P., Collicott, S.H., Schmisseur, S.H., Ladoon, D., and Randall, L.A., Munro, S.E., and Salyer, T.R., 1996, "Laminar-Turbulent Transition in the Purdue Mach 4 Quiet-Flow Ludwieg Tube," *AIAA Paper* 96-2191.

[21] Schubauer, G.B., and Skramstad, H.K, 1947, "Laminar boundary layer oscillations and stability of laminar flow," *J. Aero. Sciences*, Vol. 14, pp. 69-78.

[22] Stetson, K.F., Thompson, E.R., Donaldson, J.C., 1983, "Laminar Boundary Layer Stability Experiments on a Cone at Mach 8, Part 1: Sharp Cone ," *AIAA* Paper 83-1761.

[23] Stetson, K.F., and Kimmel, R.L., "On Hypersonic Boundary-Layer Stability," *AIAA Paper* 92-0737.

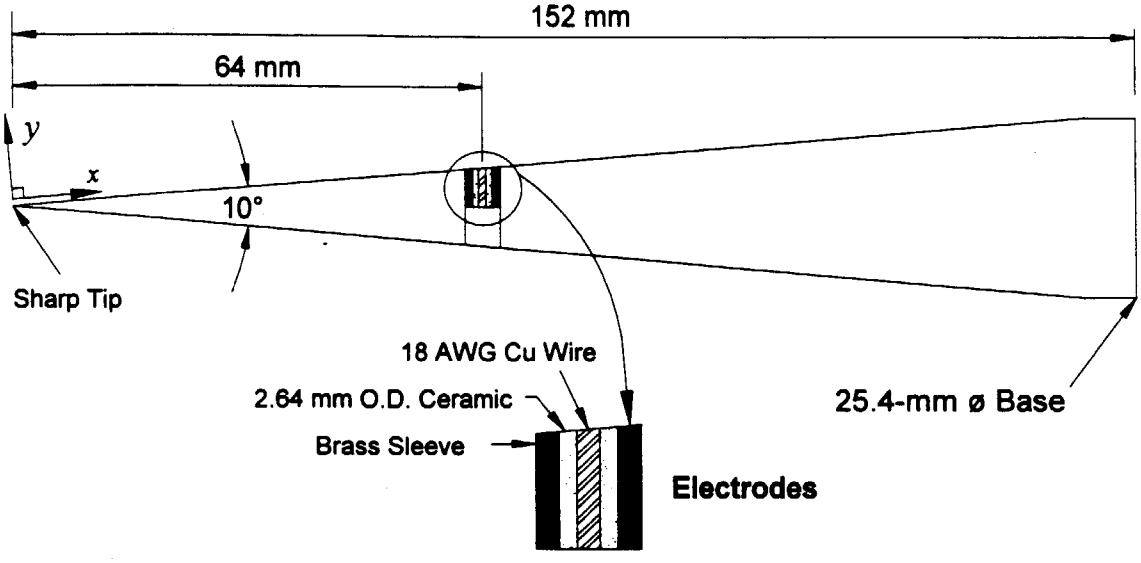

Fig. 1: 5° Cone with Glow-Discharge Perturber.

Fig. 2: Surface Glow Discharge on the 5° Cone During Mach-4 Flow.
(Flow is from right to left, ⇐)

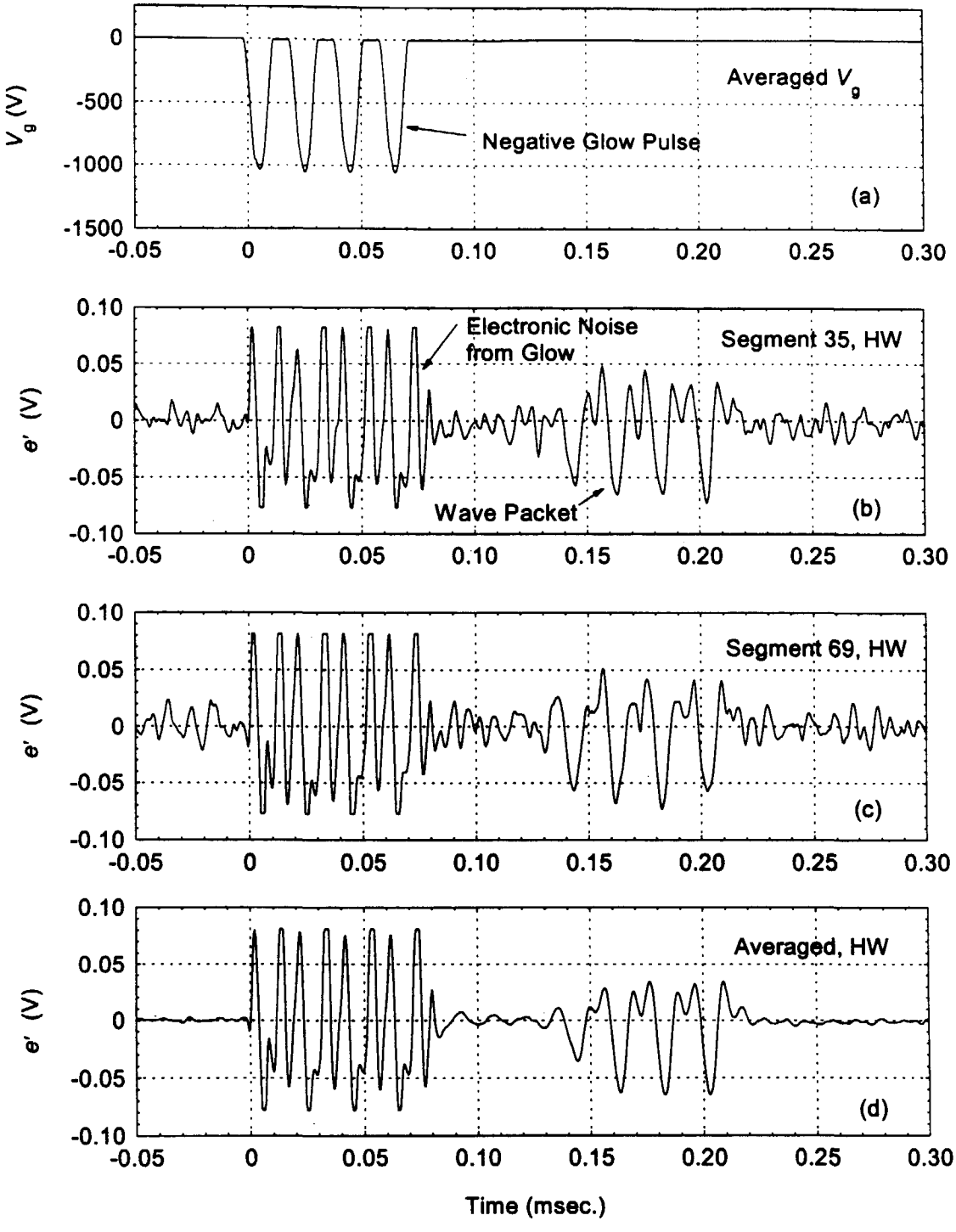

Fig. 3: *Typical Measured Traces for a Pulsed Glow Discharge: (a) Voltage Drop Across the* Electrodes, (b) and (c) Hot-Wire Fluctuations, Single Realization, and (d) Hot-Wire Fluctuations, Ensemble Averaged. 5° Cone and 3° AOA, x = 140 mm, y = 5.15 mm.

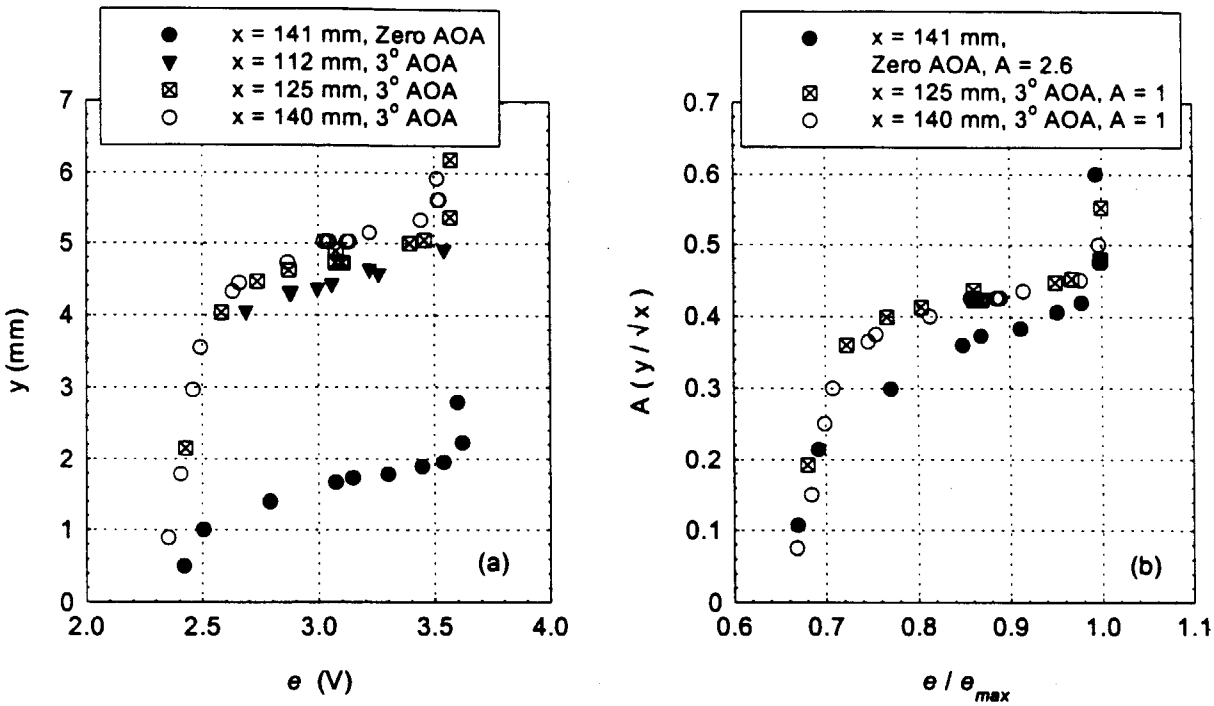

Fig. 4: Measured Mean Boundary-Layer Profiles on the 5° Cone.

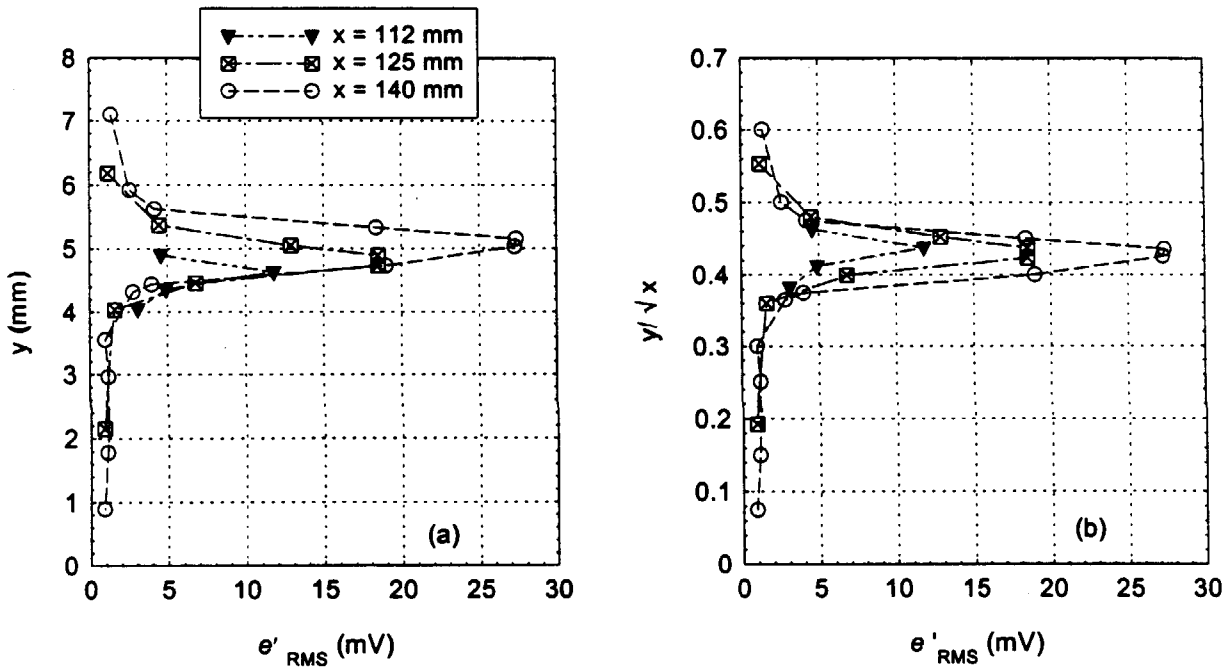

Fig. 5: Mode Shapes of the Wave Packets Generated on the 5° Cone at 3° AOA.

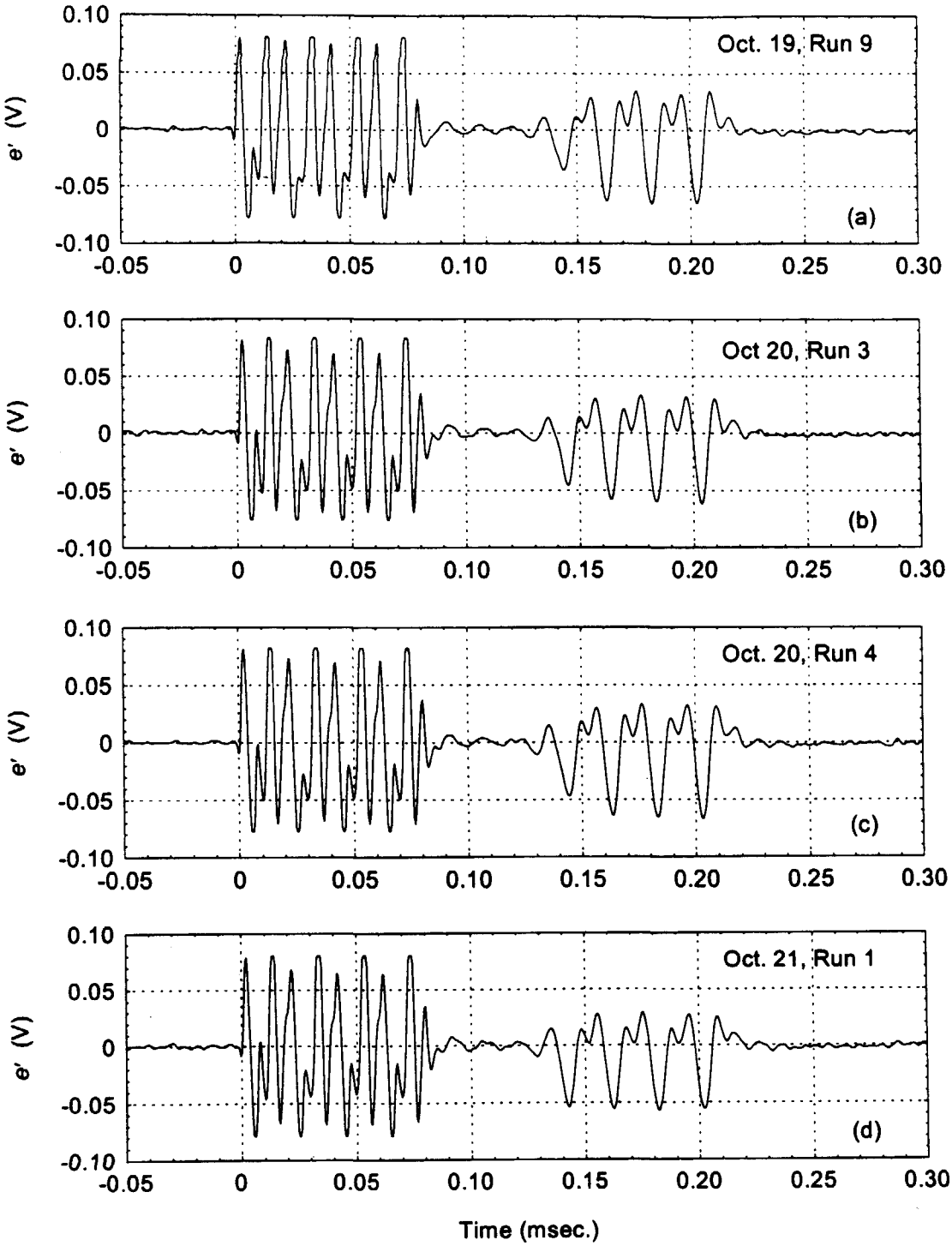

Fig. 6: Repeatability of Wave Packets at (x, y) = (140 mm, 5.03 mm).

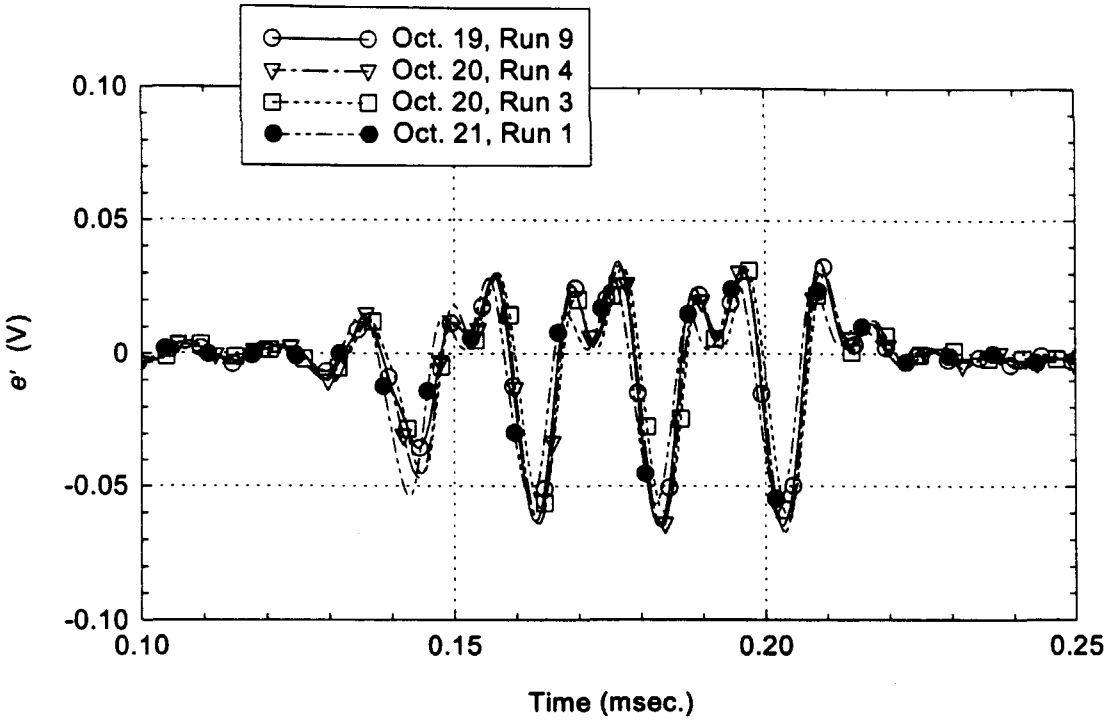

Fig.7: Comparison of Wave Packets at $(x, y) = (140 \text{ mm}, 5.03 \text{ mm})$.

Test	e'_{RMS} (mV)
Oct. 19, Run 9	27.3
Oct. 20, Run 3	25.7
Oct. 20, Run 4	28.1
Oct. 21, Run 1	26.4

Table 1: RMS Values of Wave Packets at $(x, y) = (140 \text{ mm}, 5.03 \text{ mm})$.

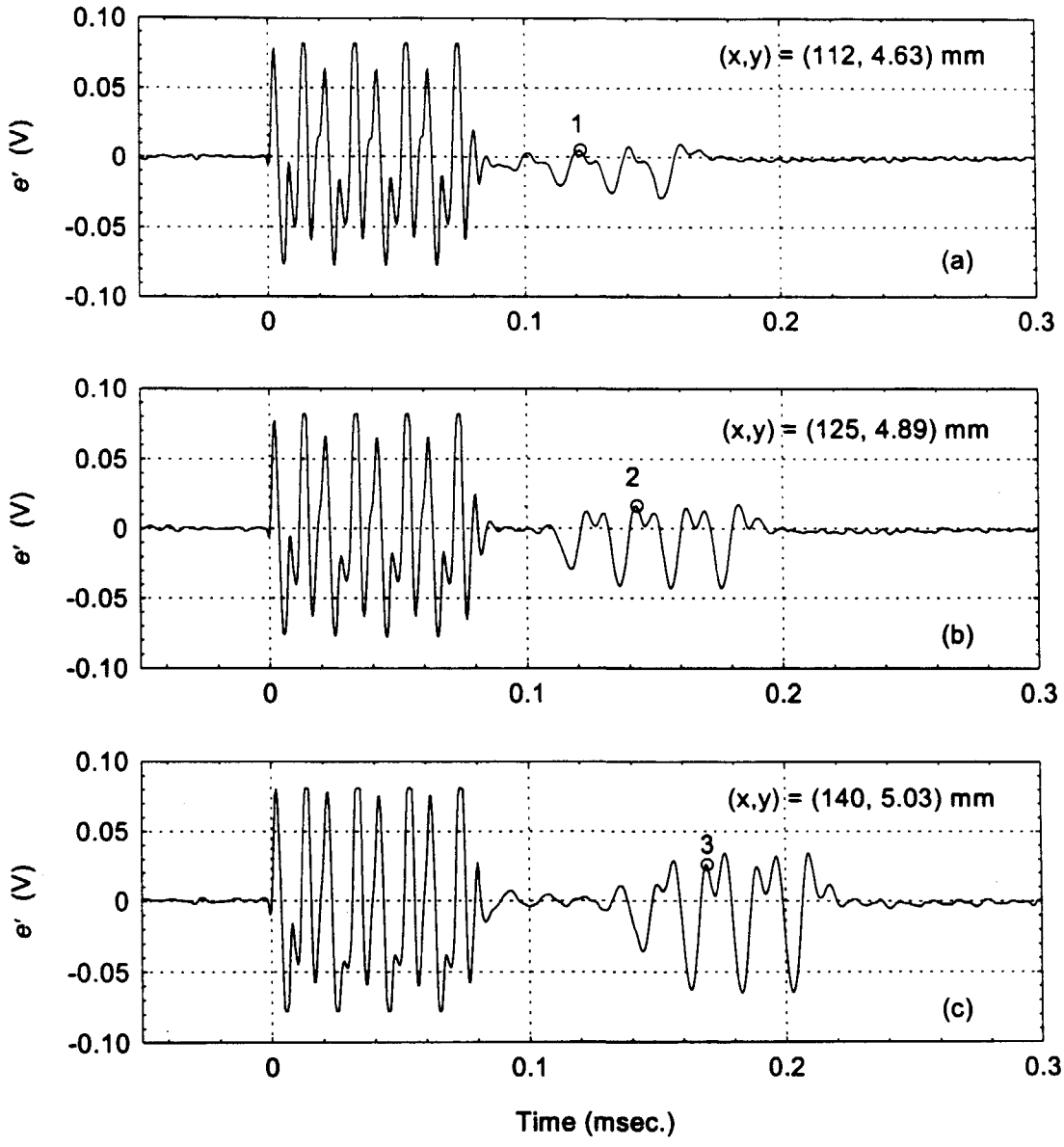

Fig. 8: Growth of a Glow-Discharge Generated Wave Packet with Downstream Distance: (a) x = 112 mm, (b) x = 125 mm, and (c) x = 140 mm. Glow Discharge at x = 64 mm.